

Otoacoustic emissions in time-domain solutions of nonlinear non-local cochlear models

Arturo Moleti and Nicolò Paternoster

Dipartimento di Fisica, Università di Roma Tor Vergata, 00133, Rome, Italy

Daniele Bertaccini

Dipartimento di Matematica, Università di Roma Tor Vergata, 00133, Rome, Italy

Renata Sisto and Filippo Sanjust

Dipartimento Igiene del Lavoro, ISPESL, 00040, Monte Porzio Catone, Rome, Italy

(Received 10 June 2009; revised 17 August 2009; accepted 17 August 2009)

A nonlinear and non-local cochlear model has been efficiently solved in the time domain numerically, obtaining the evolution of the transverse displacement of the basilar membrane at each cochlear place. This information allows one to follow the forward and backward propagation of the traveling wave along the basilar membrane, and to evaluate the otoacoustic response from the time evolution of the stapes displacement. The phase/frequency relation of the response can be predicted, as well as the physical delay associated with the response onset time, to evaluate the relation between different cochlear characteristic times as a function of the stimulus level and of the physical parameters of the model. For a nonlinear cochlea, simplistic frequency-domain interpretations of the otoacoustic response phase behavior may give inconsistent results. Time-domain numerical solutions of the underlying nonlinear and non-local full cochlear model using a large number (thousands) of partitions in space and an adaptive mesh in time are rather time and memory consuming. Therefore, in order to be able to use standard personal computers for simulations reliably, the discretized model has been carefully designed to enforce sparsity of the matrices using a multi-iterative approach. Preliminary results concerning the cochlear characteristic delays are also presented. © 2009 Acoustical Society of America. [DOI: 10.1121/1.3224762]

PACS number(s): 43.64.Jb, 43.64.Kc [BLM]

Pages: 2425–2436

I. INTRODUCTION

Otoacoustic emissions (OAEs) are a physiological by-product of the activity of the mammalian cochlea (Probst *et al.*, 1991). The OAE generation and backward transmission is effectively described by transmission line cochlear models, including tonotopically resonant transverse impedance terms (e.g., Talmadge *et al.*, 1998). These terms must also model the active feedback mechanism mediated by the outer hair cells (OHCs), which is responsible for the excellent threshold sensitivity and frequency resolution of the mammalian hearing system. A comprehensive cochlear model must be, to some extent, both nonlinear and non-local, and based on the knowledge of the OHC mechanoelectric behavior. Several models of the OHC feedback mechanism have been developed (e.g., Nobili and Mammano, 1996; de Boer and Nuttall, 2003) including detailed analyses of the OHC coupling to the basilar membrane (BM) and to the tectorial membrane, and they have been tested and refined in the past decades through comparison with experimental data, reaching a fairly high degree of complexity, and a correspondingly high number of free parameters. Most models used to predict the OAE generation adopt a simplified view of the OHC active mechanism. This attitude is partly justified by the fact that OAE generation is only a by-product of the cochlear amplifier activity, and the OAE measurable parameters may be critically dependent on cochlear transmission properties other than the details of the local cochlear ampli-

fier at the generation place(s). Nevertheless, some key properties of the OHC physiology must be retained in a full cochlear model, even if one's main purpose is getting correct predictions of the OAE phenomenology.

Nonlinearity is an intrinsic feature of the cochlear physiology, so the frequency-domain solutions of the linearized problem can only approximately predict the behavior of the system, and only in a perturbative regime. Much care must therefore be used when applying to such a system concepts that are fully meaningful for linear systems only, such as the complex frequency response, defined as the Fourier transform (FT) of the impulsive response, or the group delay, defined as the negative slope of the phase/frequency relation. The intrinsically nonlinear equations describing the cochlear micromechanics require, in a nonperturbative regime, a solution in the time domain. On the other hand, the time-domain numerical solutions may become expensive in terms of computational time and memory demanding, if sufficient spatial and time resolutions have to be achieved. High spatial resolution is necessary because the discontinuous variation in the transverse impedance parameters caused by discretization itself must not cause significant spurious reflection of the forward traveling wave (TW). High time resolution is automatically provided by the adaptive integration time step set by the routines used to solve the differential equations, and the related computational cost depends strongly not only on

the number of elements of the discretized cochlea but also on the frequency content of the stimulus and on the characteristic frequencies of the system.

Elliott *et al.* (2007) proposed a matrix formalism, applied to a finite-difference solution method of cochlear models, which is used in this study to model the propagation of the TW and the generation and backward propagation of OAEs. Elliott *et al.* (2007) originally applied this solution scheme to an active linear and local model developed by Neely and Kim (1986). In the Neely and Kim (1986) model, each micromechanical element is a two degree of freedom system of coupled oscillators, simulating some the active cochlear amplifier properties (negative resistance, or anti-damping, in a limited region close to the resonant place). The same scheme can be modified to represent several different cochlear models. In the model by Kim and Xin (2005) (adapted from Lim and Steele, 2002 and generalized to model cochlear impairment in Bertaccini and Fanelli, 2009), the forces applied by the OHCs on the BM are schematized by a nonlinear non-local feed-forward term.

In this work, a feed-forward nonlinear non-local model similar to that proposed by Kim and Xin (2005), in which the OHC additional pressure is assumed proportional to the total pressure on the BM within a slightly more basal region, is implemented in the Elliott *et al.* (2007) semidiscrete scheme, including as well random spatial variations in the impedance parameters (cochlear roughness), which are needed to get appreciable OAE response through coherent reflection (Talmadge *et al.*, 1998), acting as backscattering centers for the forward TW. The semidiscrete model is then fully discretized, and the resulting discrete model is solved efficiently. A nontrivial mass matrix and stiffness of the BM micromechanics (in the numerical analysis sense, i.e., the presence of high Lipschitz constants in the nonlinear model) are suggested using an implicit time-step integrator. Therefore, at each time step, a large system of fully coupled nonlinear algebraic equations should be solved in order to generate the numerical approximations, and this is computationally expensive. In this work, an efficient and reliable numerical simulation is enforced by decoupling the differential part of the discretization of the integrodifferential model by solving sparse linear systems using multi-iterative projection algorithms instead of inverting matrices. A graphical user interface has been added to facilitate the parameters inputted and the analysis of the results. The backward TW associated with OAEs is observed as a displacement wave at the stapes, and some properties of the otoacoustic delays are analyzed.

A variation in the above model was also considered, in which the feed-forward coupling is obtained assuming that the OHC additional pressure is directly proportional to the BM velocity. In this model, this additional force explicitly behaves as a simple anti-damping term.

This discrete model, implemented in our package, after its necessary optimization through comparison with the available data, could be a useful tool to design future OAE experiments, predicting the OAE response at different stimulus levels, and, in particular, to study in more detail the gen-

eration place and time of the different components of the OAE response, as well as their direction of propagation along the BM.

In Sec. II, we recall the physical meaning of the cochlear characteristic times that are estimated with different experimental techniques. In Sec. III A we briefly describe the application of Elliott's solution scheme to a very simple one-dimensional (1D) linear, passive, and local cochlear model, to help the reader through Sec. III B, where we discuss its generalization to more realistic, still semidiscrete models, including feed-forward nonlinear and non-local terms. In Sec. III C, we propose a fully discrete feed-forward analog of the underlying model and notes concerning its implementation in the MATLAB environment. In Sec. IV, we discuss our preliminary results, focusing on the relation between different characteristic times in a nonlinear cochlea.

II. BACKGROUND ON COCHLEAR DELAYS IN MODEL AND EXPERIMENT

The study of the characteristic times of the OAE response may provide important information about the cochlear mechanics and the otoacoustic generation mechanisms, complementing other measures coming, e.g., from direct observations of the BM vibration (Ren, 2004; He *et al.*, 2007) and from the analysis of the auditory brainstem response (ABR) (e.g., Neely *et al.*, 1988; Donaldson and Ruth, 1993).

A. TEOAE latency from time-frequency analysis and cochlear transmission delay

In the case of transient evoked OAEs (TEOAEs) and, particularly for click-evoked OAEs (CEOAEs), the latency may be defined in the time domain as the interval between the impulsive stimulus and the onset of the otoacoustic response at a given frequency, which can be measured using time-frequency analysis techniques, based on the wavelet transform or on the MATCHING PURSUIT algorithm (Tognola *et al.*, 1997; Sisto and Moleti, 2002; Jedrzejczak *et al.*, 2004). As the middle ear roundtrip transmission introduces only a very short time delay, of order 0.1–0.2 ms (Puria, 2003; Voss and Shera, 2004), the OAE latency is almost entirely of cochlear origin, being associated for each frequency with the time needed to transmit forward the stimulus from the cochlear base to each tonotopic place as a TW, and backward to the base. This delay is a function of the geometrical and mechanical characteristics of the BM, including those of active filter associated with the feedback mechanism that is mediated by the OHCs. The tonotopic structure of the BM causes the overall decrease in latency with increasing frequency, simply because the cochlear round trip path is longer for lower frequencies. The frequency selectivity of the active cochlear filter is also related to the OAE delay, which increases by increasing the tuning factor Q of the resonance. As a consequence, the OAE latency is a decreasing function of both frequency and stimulus level (Sisto and Moleti, 2007). This property has also been found in the wave-V ABR delay, which is made up (Eggermont and Don, 1980; Neely *et al.*, 1988; Don *et al.*, 1993; Donaldson and Ruth, 1993;

Abdala and Folsom, 1995) of a constant term of neural origin (this is surely true for its main contribution, the delay between wave-I and wave-V), independent of frequency and stimulus level, and of a cochlear term, decreasing with increasing frequency and stimulus level, which is evidently associated with the forward cochlear transmission delay.

Transmission line cochlear models (Furst and Lapid, 1988; Talmadge *et al.*, 1998; Shera *et al.*, 2005) are usually in agreement in representing the acoustic signal propagation along the BM as a TW. Due to the tonotopicity of the BM, each Fourier component of the stimulus propagates up to its resonant place, where it produces the maximum transversal displacement of the BM, associated with that tone perception, and then it is locally absorbed.

B. OAE generation mechanisms

It is generally accepted that OAEs are produced by two different mechanisms: nonlinear distortion and linear reflection (Shera and Guinan, 1999).

The cochlear response nonlinearity generates distortion at moderate and high BM excitation levels. A threshold for the onset of nonlinearity can be fixed at some transverse displacement amplitude of order 10 nm. At these stimulus levels, significant OAE generation is expected from the nonlinear generation mechanism. If a given cochlear region is simultaneously excited by two tones of different frequencies, the system nonlinearity also produces tones at frequencies that are linear combinations of those of the stimulus, as in the case of the distortion product OAEs (DPOAEs). The nonlinear distortion generation always occurs at the tonotopic cochlear place of the stimulus frequency, or, as in the DPOAE case, in a place that is a well-defined function of the frequencies of the stimulus (primary tones); this generation mechanism is therefore called “wave-fixed” (Shera and Guinan, 1999). Linearized transmission line cochlear models (Talmadge *et al.*, 1998, 2000; Shera *et al.*, 2005), solved in the frequency domain, predict for OAEs generated by wave-fixed mechanisms a flat phase spectrum (at least, in the scale-invariant limit). If the resulting null “group delay” were simplistically interpreted as instantaneous cochlear response, there would be obvious contradiction with the hypothesis that the otoacoustic response is generated at (or near) the tonotopic place, for each frequency, because at least the forward propagation of the stimulus (one could argue that the backward OAE propagation could be much faster) would need a significant and well-measurable transmission time, from a few to several milliseconds, dependent on frequency.

OAE generation is also expected to be associated with the reflection of a significant fraction of the forward TW. It is necessary to postulate the presence of randomly distributed microirregularities of the cochlear mechanical structure, which act as backscattering centers for the forward TW (Zweig and Shera, 1995). Perturbative estimates of the cochlear reflectivity, based on the osculating parameters technique (Shera and Zweig, 1991; Talmadge *et al.*, 2000), suggest that most of the linearly reflected wave should come from a region close to the resonant place. Recent estimates based on a linear model by Choi *et al.* (2008) suggest instead

that a significant contribution to the overall SFOAE response may come from cochlear regions remote from the resonant place. Coherent reflection from a rather broad cochlear region slightly basal to the resonant place is predicted by the coherent reflection filtering (CRF) theory, which also introduces time-delayed stiffness terms in the BM micromechanics to get the necessary tall and broad activity pattern. These “Zweig” terms, due to their rather fine-tuned delays, act as effective damping and anti-damping terms in that cochlear region, providing the negative resistance region required by the solution of the inverse cochlear problem applied to experimental BM transfer function data. As already remarked, similar results could be obtained with different mathematical approaches, e.g. modeling each cochlear partition as a two degree of freedom system of linear actively coupled oscillators (Neely and Kim, 1986), or by introducing active non-local terms. In the CRF theory, the OAE generation mechanism is considered “place-fixed” because the backscattering centers are localized at fixed positions. The CRF theory predicts, for such a place-fixed mechanism, a rapidly rotating phase spectrum (Talmadge *et al.*, 1998; Shera *et al.*, 2005). The additional reflection from more basal cochlear regions suggested by Choi *et al.* (2008) would imply a flatter phase-frequency relation, and the vector superposition of the two sources would explain the observed stimulus-frequency OAE (SFOAE) spectral fine structure, without having to assume contributions from nonlinear distortion.

C. Relation among different cochlear characteristic times

Much experimental evidence has been gathered about the relation among different cochlear characteristic times. A general warning applies to such comparisons. In classical BM transfer function measurements (e.g., Rhode, 1971), the place of measurement is fixed as the frequency changes. The phase slope represents a partial derivative. In OAE experiments, this is not generally the case. The relation between OAE phase-gradient delays and the actual time delay of each frequency component of the OAE response is not straightforward, and depends on the wave-fixed or place-fixed nature of the OAE generator. OAE phase-gradient delays are actually measured by computing the slope of the phase-frequency relation, but the phase is a function of both the frequency of the OAE and the position of the source. The experimentally measured slope is therefore a total derivative, which includes an additional term for wave-fixed generation, which almost totally cancels, in the WKB approximation (Sisto *et al.*, 2007), the one associated with the roundtrip transmission delay. For place-fixed generation, instead, the phase is a function of frequency only, and the phase-gradient delay is therefore expected to approximately coincide with the physical transmission delay.

At low stimulus levels, the OAE response should be dominated by linear place-fixed mechanisms, the SFOAE phase-gradient delay is therefore expected to be closely related to the physical delay associated with the forward and backward transmissions along the BM. Early applications of the CRF theory predicted indeed that the SFOAE phase-gradient delay is twice the BM group delay (Shera and

Guinan, 2003), while refined calculations (Shera *et al.*, 2005) concluded that the phase-gradient delay should be slightly less than twice the BM group delay.

Accurate studies on chinchillas (Siegel *et al.*, 2005) demonstrated that the SFOAE phase-gradient delay is significantly less than twice the BM group delay, particularly at low-frequency. This result has been considered in agreement with the CRF theory assuming that some contribution from nonlinear distortion is also present in the SFOAE response (Shera *et al.*, 2006). Another explanation of these discrepancies could be provided by the linear reflection sources remote from the resonance place proposed by Choi *et al.* (2008). It has also been shown (Sisto *et al.*, 2007) that the roundtrip cochlear delay measured by time-frequency analysis of CEOAE waveforms closely matches the phase-gradient delay of the same OAE spectra, at click stimulus levels from 60 to 90 dB peak SPL (pSPL), concluding that linear reflection from roughness is the main source of TEOAEs in this stimulus level range. We recall that the pSPL level of a click is given by the ratio between its peak amplitude and the standard reference pressure level (20 μ Pa), expressed in decibels. The associated spectral density is a function of the click duration.

For DPOAEs, the relation between latency, phase-gradient delay, BM group delay and frequency is even less straightforward, and depends on the experimental sweeping paradigm (Prijs *et al.*, 2000; Schoonhoven *et al.*, 2001). If the ratio f_2/f_1 is kept constant, from the solution of the linearized cochlear equations (Talmadge *et al.*, 2000), it follows that the nonlinear distortion component, originated in $x(f_2)$, should have flat phase spectrum, while the linear reflection source coming from $x(f_{DP})$ should give a contribution with rapidly rotating phase. In the time domain, it is clear that the nonlinear generation may start only after the transmission time needed for the f_1 and f_2 tones to reach the nonlinear generation place $x(f_2)$. After that, an additional (shorter) time is necessary for the backward TW at frequency f_{DP} to reach the base. The backward delay is shorter because the wave packet of frequency f_{DP} moves away from a region that is already more basal than its tonotopic region, where its group velocity would be considerably lower (Moleti and Sisto, 2003) (this slowing-down effect near the resonant place is sometimes called “filter build-up time,” it may be seen as a significant contribution to the path integral of the inverse velocity coming from a rather short part of the path). The second DPOAE source [from linear reflection at $x(f_{DP})$] is significantly more delayed because the distortion tone generated in $x(f_2)$ must reach its own tonotopic place $x(f_{DP})$ to be amplified and reflected back by roughness. Therefore, its overall onset delay in the time domain is expected to be close to the latency of the component of frequency f_{DP} of a correspondently high TEOAE response [neglecting the dependence on the stimulus level, which makes a little shorter the forward transmission delay to $x(f_2)$ of the primary tones f_1 and f_2 , due to their higher level]. Summarizing, observing the phase of the two DPOAE components in the frequency domain, one should see a flat phase component and a rotating phase component (which can be separated using time-domain filtering), whereas observing the onset of the re-

sponse in the time domain, one should observe an early (but not instantaneous) response from the first source and a more delayed onset of the linear reflection contribution. Long *et al.* (2008) recently exploited the different phase behaviors of the two DPOAE components to separate them by using sufficiently fast-sweeping primary tones. Whitehead *et al.* (1996) were able to measure (in humans and rabbits) the onset time of DPOAEs elicited by high-level primaries [75 dB sound pressure level (SPL)] using a clever differential acquisition technique based on phase rotation of the primary tones. They measured delays from 2 to 5–10 ms (depending also on the data analysis algorithm) in the 1–8 kHz range, with the expected frequency dependence. These delays are compatible with those expected from the nonlinear distortion source, which should be dominant at high stimulus levels.

D. OAE backward propagation

By comparing the OAE latency to the ABR wave-V latency in the same stimulus level range, it has been shown that the part of the ABR latency that is independent of frequency and stimulus level (associated with the forward cochlear path of the stimulus) is approximately equal to half the OAE latency (Moleti and Sisto, 2008), supporting the hypothesis that the backward propagation of OAEs is due to a slow transverse TW on the BM. This conclusion is in agreement with analyses of the data from Allen–Fahey experiments (Shera *et al.*, 2007), and with direct measurements by Dong and Olson (2008), but it is contradicted by the slope of the DP phase at different cochlear places measured by accurate observations of the BM vibration either by moving the observation place (He *et al.*, 2007) or by moving the primary frequencies (de Boer *et al.*, 2008). These contradictory observations could be attributed to a dominant forward traveling DP within the cochlea, which would obscure the observation of reverse waves.

The above list of interesting issues, which can only be approximately evaluated with frequency-domain solutions, due to the intrinsic nonlinearity of the problem, was meant to demonstrate the strong need for time-domain solutions of the full cochlear problem. In the following, we will discuss some preliminary results from the time-domain solution of a nonlinear non-local active cochlear model, focusing on possible applications to the study of the OAE delays.

III. COCHLEAR MODELS

A. Linear 1D box model

In this subsection, we apply the scheme of Elliott *et al.* (2007) to a very simple linear passive model, to help the reader getting through the formalism before going to Sec. III B, where the feed-forward model is described. A list of the parameter values used in the model is reported in Table I.

For an incompressible fluid, in a cochlear duct of rectangular constant cross section of constant half-height H and length L , divided by a tonotopically resonant elastic BM, the wave propagation along the cochlea on the BM ($z=0$), reduces to the 1D transmission line equation for the differential pressure p :

TABLE I. Model parameters used in this study. Some of the parameter values listed below are taken from [Talmadge et al. \(1998\)](#), they are indicated by (T98).

Parameter	Value	Definition
ρ	10^3 kg m^{-3}	Fluid density
L	$3.5 \times 10^{-2} \text{ m}$	Length of the BM
k_0	$3.1 \times 10^3 \text{ m}^{-1}$	Cochlear geometrical wavenumber (T98)
ω_0	$2.08 \times 10^4 \cdot 2\pi \text{ s}^{-1}$	Greenwood's map frequency coefficient (T98)
σ_{bm}	$5.5 \times 10^{-2} \text{ kg m}^{-2}$	BM density (T98)
ω_1	$-145 \cdot 2\pi \text{ s}^{-1}$	Greenwood's map frequency offset (T98)
k_ω	$1.382 \times 10^2 \text{ m}^{-1}$	Greenwood's map inverse length scale (T98)
γ_0	$5.035 \times 10^3 \text{ s}^{-1}$	Cochlear damping map coefficient (T98)
γ_1	100 s^{-1}	Cochlear damping map offset (T98)
k_Γ	$1.382 \times 10^2 \text{ m}^{-1}$	Cochlear damping map inverse length scale (T98)
K_{ow}	$2 \times 10^8 \text{ N m}^{-3}$	Effective middle ear-oval window stiffness
γ_{ow}	$5 \times 10^3 \text{ s}^{-1}$	Effective middle ear-oval window damping
σ_{ow}	2 kg m^{-2}	Effective middle ear-oval window density
ξ_{nl}	10^{-8} m	OHC gain saturation length scale
γ	0.36	OHC gain parameter
λ	$1.2 \times 10^{-7} \text{ m}^2$	OHC non-local interaction range (squared)

$$\frac{\partial^2 p(x, 0, t)}{\partial x^2} = \frac{2\rho}{H} \ddot{\xi}(x, t), \quad (1)$$

where ρ is the fluid density and ξ is the BM transverse displacement at the longitudinal position x and time t .

Equation (1) is obtained, as usual, assuming the fluid incompressibility, using the boundary condition on the BM:

$$\left. \frac{\partial p(x, z, t)}{\partial z} \right|_{z=0} = 2\rho \ddot{\xi}(x, t), \quad (2)$$

and that on the rigid upper wall:

$$\left. \frac{\partial p(x, z, t)}{\partial z} \right|_{z=H} = 0. \quad (3)$$

As in [Elliott et al., 2007](#), the first of the N elements of the semidiscretized model includes the middle ear dynamics and the boundary condition for the wave equation (1) at the basal end:

$$\left. \frac{\partial p}{\partial x} \right|_{x=0} = 2\rho \ddot{\xi}_{ow}, \quad (4)$$

where $\ddot{\xi}_{ow}$ is the acceleration of the stapes. [Elliott et al. \(2007\)](#) wrote this acceleration as the linear combination of two components: the acceleration due to external excitation and that due to the loading by the internal pressure response in the cochlea at $x=0$. We prefer to choose a slightly different approach, putting the term associated with the stimulus in the ear canal as a forcing term in the dynamical equation for the first element of the partition, according to Eq. (10) of [Talmadge et al., 1998](#):

$$\ddot{\xi}_{ow}(t) + \gamma_{ow} \dot{\xi}_{ow}(t) + \omega_{ow}^2 \xi(t) = \frac{p(0, t) + G_{me} P_{dr}(t)}{\sigma_{ow}}, \quad (5)$$

where, γ_{ow} , $K_{ow} = \omega_{ow}^2 \sigma_{ow}$, and σ_{ow} are the phenomenological parameters reported in Table I, chosen to represent the filtering properties of the middle ear, P_{dr} is the calibrated pressure in the ear canal (for a rigid ear drum), and G_{me} is the middle ear mechanical gain of the ossicles.

The last element of the spatially discretized cochlea is the helicotrema, which is described, as usual, by a pressure release (short-circuit) boundary condition:

$$p(L, z, t) = 0. \quad (6)$$

Considering the dynamical equation that relates the BM transversal displacement to the p acting on the tonotopic oscillator, we have for the elements from 2 to $N-1$:

$$\ddot{\xi}(x, t) + \gamma_{bm}(x, \xi, \dot{\xi}) \dot{\xi}(x, t) + \omega_{bm}^2(x, \xi, \dot{\xi}) \xi(x, t) = \frac{p(x, 0, t)}{\sigma_{bm}}. \quad (7)$$

The height H is related to the BM density and to the cochlear geometrical wavenumber k_0 , defined in [Talmadge et al., 1998](#) by $H = 2\rho/k_0^2 \sigma_{bm}$.

In the simplest form of the model, each tonotopic place is schematized by a single passive oscillator, and both damping and stiffness are smooth functions of the x only, according to the Greenwood map ([Greenwood, 1990](#)):

$$\begin{aligned} \omega_{bm}(x) &= \omega_0 e^{-k_\omega x} + \omega_1, \\ \gamma_{bm}(x) &= \gamma_0 e^{-k_\Gamma x} + \gamma_1. \end{aligned} \quad (8)$$

In the limit $k_\Gamma = k_\omega$, and $\omega_1 = \gamma_1 = 0$, the map is also scale-invariant. This symmetry is violated in the real cochlea, particularly at low-frequency, due to the constant terms ω_1 and γ_1 , and also because $k_\Gamma \neq k_\omega$. Indeed, cochlear tuning $Q = \omega/\gamma$ increases with frequency, as shown by behavioral and otoacoustic data (e.g., [Glasberg and Moore, 1990](#); [Shera et al., 2002](#); [Unoki et al., 2007](#); [Sisto and Moleti, 2007](#)).

[Elliott et al. \(2007\)](#) described each element of the cochlear partition as a system of two coupled linear oscillators, including active terms, according to a model by [Neely and Kim \(1986\)](#). In this study, we chose a different approach, describing each partition with a single oscillator, and introducing, in the next subsection, active amplification and non-linear saturation terms as additional forces triggered by the OHCs and acting on the BM, generated by non-local feed-forward longitudinal interaction, similar to what has been proposed by [Kim and Xin \(2005\)](#), see also [Bertaccini and Fanelli, 2009](#), in different solution schemes.

Using finite-difference approximation for the spatial derivatives, the semidiscrete models can be written in matrix form

$$FP(t) = \ddot{\Xi}(t), \quad (9)$$

where F is Elliott's $N \times N$ finite-difference matrix, whose first and last lines include, respectively, the boundary conditions, Eqs. (4) and (6), $P(t)$ and $\ddot{\Xi}(t)$ are the N -dimensional

vectors of the differential pressure and cochlear partition acceleration, respectively:

$$F = \frac{H}{2\rho(\Delta x)^2} \begin{bmatrix} -\frac{\Delta x}{H} & \frac{\Delta x}{H} & 0 & & 0 \\ 1 & -2 & 1 & 0 & 0 \\ 0 & 1 & -2 & 1 & 0 \\ & & \dots & 1 & -2 & 1 & 0 \\ & & & & 1 & -2 & 1 \\ 0 & & & & & 0 & -\frac{2\rho(\Delta x)^2}{H} \end{bmatrix}, \quad (10)$$

where $\Delta x = x_i - x_{i-1} = L/(N-3)$.

As in Elliott *et al.*, 2007, we cast the dynamic variables $[\dot{\xi}_j(x_j, t), \xi_j(x_j, t)]$ of the micromechanical elements in a single vector of state variables U of dimension $2N$.

Equations (4)–(7) can be written for the whole set of discrete tonotopic oscillators in the form of combined matrix equations:

$$\dot{U}(t) = A_E U(t) + B_E (P(t) + S(t)), \quad (11a)$$

$$\ddot{\Xi}(t) = C_E U(t), \quad (11b)$$

where $S(t)$ is a vector whose only non-null element is the first one, which is equal to $G_{me} P_{dr}(t)$.

The matrices A_E ($2N \times 2N$), B_E ($2N \times N$), and C_E ($N \times 2N$) are block diagonal. In particular, each block A_i of the matrix A_E , for $i=2, \dots, N-1$, contains the dynamics of the i th resonant tonotopic oscillator:

$$A_E = \begin{bmatrix} A_1 & & \\ & \dots & \\ & & A_N \end{bmatrix} \quad (\text{the same rule applies to } B_E \text{ and } C_E), \quad (12)$$

with

$$\begin{aligned} A_i &\equiv \begin{bmatrix} -\gamma_{bm}(x_i) & -\omega_{bm}^2(x_i) \\ 1 & 0 \end{bmatrix}, & B_i & \\ &\equiv \begin{bmatrix} 1 & 0 \\ \sigma_{bm} & 0 \end{bmatrix}^T & \text{for } i=2, \dots, N-1, & \\ A_1 &\equiv \begin{bmatrix} -\gamma_{ow} & -\omega_{ow}^2 \\ 1 & 0 \end{bmatrix}, & B_1 &\equiv \begin{bmatrix} 1 & 0 \\ \sigma_{ow} & 0 \end{bmatrix}^T, & A_N & \\ &\equiv 0, & B_N &\equiv 0, & & \\ C_i &\equiv [1 \ 0]. & & & & \end{aligned} \quad (13)$$

The finite-difference matrix F is invertible, so we can write Eq. (9) as

$$P(t) = F^{-1} \ddot{\Xi}(t) = F^{-1} C_E \dot{U}(t). \quad (14)$$

Substituting Eq. (14) into Eq. (11a), the overall state space equation with distributed micromechanics and boundary conditions can be written in the general form

$$M_{lin} \dot{U}(t) = A_E U(t) + B_E S(t), \quad (15)$$

where M_{lin} is the $2N \times 2N$ mass matrix of the system:

$$M_{lin} = I - B_E F^{-1} C_E. \quad (16)$$

B. Nonlinear feed-forward model

In a more advanced model, the OHCs-BM interaction can be schematized as a nonlinear, non-local active system that can be included into the same matrix solution scheme.

In the model by Kim and Xin (2005), the pressure applied by OHCs on the BM is assumed proportional to the total pressure on the BM, and, due to the longitudinal tilt of OHCs, forces acting on the cilia at x cause OHCs to push at a point $x+\Delta$ downstream on the BM:

$$q(x+\Delta, t) = \alpha(\xi, x, t) p_{BM} = \alpha(\xi, x, t) (p(x, t) + q(x, t)), \quad (17)$$

where q is the additional pressure given by the OHCs, p_{BM} is the total pressure on the BM, and α is a nonlinear non-local gain factor, which depends on the BM displacement ξ in a cochlear region around the considered position x .

For the gain function, we use the integral expression (Kim and Xin, 2005):

$$\alpha(x, \xi, t) = \frac{\gamma}{\sqrt{\lambda} \pi} \int_0^L \exp\left(-\frac{(x-x')^2}{\lambda}\right) g(\xi(x', t)) dx', \quad (18)$$

where γ is a dimensionless parameter controlling the strength of the non-local terms, and $\sqrt{\lambda}$ is a characteristic length (a constant in a scale-invariant cochlea), representing the longitudinal range of the non-local interaction.

Here we choose the nonlinear analytical gain function $g(\xi(x, t))$:

$$g(\xi(x, t)) = \tanh\left(\frac{\xi_{nl}^2}{(\xi(x, t) - \xi_0)^2}\right), \quad (19)$$

which approximately matches the nonlinear gain function shown by Kim and Xin (2005) and by Lim and Steele (2002), where ξ_{nl} is a transverse BM displacement scale for the nonlinear saturation of the OHC gain, and ξ_0 is a parameter controlling the vertical asymmetry of the OHC gain (in our simulations $\xi_{nl} = 10^{-8}$ m and $\xi_0 = 0$). This is surely an oversimplified version of the actual physiology of the OHC mechanism, which is much more accurately described elsewhere (e.g., Nobili and Mammano, 1996). The inclusion of a more realistic description of the OHC physiology, which would increase the complexity of the numerical solution of the problem and would also introduce a much higher number of parameters, is beyond the scope of the present study.

Including Eq. (17), Eq. (7) is modified as follows:

$$p(x, t) + q(x, t) = \ddot{\xi}(x, t) + \gamma_{bm}(x) \dot{\xi}(x, t) + \omega_{bm}^2(x) \xi(x, t),$$

$$q(x, t) = \alpha(x - \Delta, \xi, t) (p(x - \Delta, t) + q(x - \Delta, t)) \quad (\text{for } \Delta \leq x \leq L),$$

$$q(x,t) = 0 \quad (\text{for } 0 \leq x \leq \Delta). \quad (20)$$

In the semidiscrete model, the feed-forward term is related to the pressure by

$$q(x_i,t) - \alpha(x_{i-K},\xi,t)q(x_{i-K},t) = \alpha(x_{i-K},\xi,t)p(x_{i-K},t), \quad (21)$$

where K is an integer number such that

$$\Delta = K\Delta x. \quad (22)$$

Equation (24) can be expressed as a matrix equation:

$$BQ(t) = CP(t). \quad (23)$$

$Q(t)$ and $P(t)$ are, respectively, the column vectors for $q(x_i,t)$ and $p(x_i,t)$. The matrix B has 1's on its diagonal and off-diagonal nonzero elements:

$$B(i+K,i) = -\alpha(x_i,\xi,t) \quad \text{for } i = 2, \dots, N-K. \quad (24)$$

The matrix C is a matrix whose nonzero elements are

$$C(i+K,i) = \alpha(x_i,\xi,t) \quad \text{for } i = 2, \dots, N-K. \quad (25)$$

The B and C matrices are both functions of the BM displacement. In particular, B is invertible.

After some manipulations, it can be shown that the following equation for the state vectors U holds

$$M_{nl}\dot{U}(t) = A_E U(t) + B_E S(t), \quad (26)$$

where the nonlinear mass matrix is

$$M_{nl} = (I - B_E G(U) F^{-1} C_E), \quad (27)$$

and $G(U)$ is the $N \times N$ gain matrix:

$$G(U) = B^{-1} C + I. \quad (28)$$

In the limit in which the nonlinear coupling term α is zero, the matrix B reduces to the identity matrix and C is zero. In this limit the gain matrix, $G(U)$ is coincident with the identity matrix. This is the limit in which the linear passive equations hold, Eq. (26) reduces to Eq. (15), and the mass matrix of the system reduces to M_{lin} [Eq. (16)]. For $\alpha \neq 0$, in the case $K=0$, there is no feed-forward asymmetry, but the model is still nonlinear and non-local. Different values of K could be chosen, providing the desired amount of asymmetry, to match the experimentally measured shape of the BM activity patterns.

The same scheme could be easily adapted to describe different models of the OHC function. For example, one could assume that the additional OHC pressure is proportional to the BM velocity. This assumption may be questionable on a physiological basis, but it is, however, interesting to note that it would lead to a model in which the OHC force would act as an explicit anti-damping term everywhere along the BM, not only near the resonant place. As this assumption is implicitly made, when one uses simple 1D transmission line models in which the anti-damping term is just a negative damping constant at each cochlear place and saturation is given by a quadratic damping term (e.g., a Van der Pol oscillator model), it could be interesting to compare the time behavior of OAEs produced by such a model with that predicted by the previous one.

Equation (21) would formally change to

$$q(x_i,t) = \alpha'(x_{i-K},t)\sigma_{bm}\gamma_{bm}(x_i)\dot{\xi}(x_{i-K},t), \quad (29)$$

where $\gamma(x_i)$ is the local damping constant and α' is obtained from an integral like that of Eq. (18), with a different value γ' of the dimensionless constant γ that controls the stability of the resonance.

The mass matrix of Eq. (27) becomes

$$M'_{nl} = I - B_E(F^{-1}C_E + CD_E), \quad (30)$$

where D_E is a block diagonal matrix, whose elements are

$$D_{i>1} = [0 \quad \sigma_{bm}\gamma_{bm}(x_i)], \quad D_1 = [0 \quad 0], \quad (31)$$

whereas the other matrices are unchanged.

If the nonlinear gain function $g(\xi(x,t))$ is also changed to

$$g'(\xi(x,t)) = 1 - \frac{\xi^2}{\xi_{nl}^2}, \quad (32)$$

one gets a nonlinear non-local model with explicit anti-damping and quadratic nonlinear damping at each cochlear place x :

$$\gamma'(x,\xi) = \gamma_{bm}(x) \left(-\alpha' + 1 + \alpha' \frac{\xi^2}{\xi_{nl}^2} \right). \quad (33)$$

We note that the generalization to a wide class of different models is a simple task, in the scheme of Elliott *et al.* (2007), exploiting the fact that one is free to select the BM velocity as the first component of each element of the state vector U or as the second component of each element of U using the matrices C_E and D_E , respectively. This freedom of choice is important because it allows one to put the nonlinear term into the mass matrix of the system.

C. A fully discrete nonlinear active model and its numerical implementation

In this section, we discuss a numerical approximation technique for the *semidiscrete* model (26). We recall that semidiscrete means that we have to do it with a model that is no longer based on partial differential equations, still continuous, but now only ordinary derivatives are present. We consider a uniform mesh on a rectified model of the BM. Discretization with respect to the spatial variable x imposed on the BM gives the sequence of systems of nonlinear integrodifferential equations (26), (18), and (19) with null initial conditions, where each of the systems as in Eq. (26) is parametrized by the spatial step Δx of the mesh. We recall that the integral part of both the continuous and the semidiscrete model (26) is due to the nonlocality of the gain factor $\alpha(\xi,x,t)$ in Eq. (18) and hidden in the matrix functions B , C , and $G(U)$ in Eq. (26), computed for each time step. In order to simplify the overall calculation and to avoid potential instabilities, we computed the gain factor by using information from the previous step; i.e., we considered a sort of semi-implicit reduction of the models (26), (18), and (19).

We remark that the differential systems in Eq. (26) have a nontrivial mass matrix whose expression can be simplified in

$$M_{nl} = I - B_E B^{-1} F^{-1} C_E, \quad (34)$$

by using Eq. (28) and observing that $C = -B + I$; i.e., the expression of the gain matrix can be reduced to $G(U) = B^{-1}$.

In order to provide time-step integration of Eq. (26), we observe that, whenever the mass matrix is different from the identity, using a package based on implicit or on explicit formulas has similar computational costs. In particular, in order to advance in time, one needs to solve algebraic nonlinear equations requiring the solution of algebraic linear systems of neq equations, where neq is the number of single differential equations in Eq. (26) even using a code based on explicit formulas. Therefore, we modified for the use of a multi-iterative procedure a stable package based on Backward Differentiation Formulas (BDF-like) variable step, variable order (from order 1 to 5) formulas that are of implicit type, `ode15s`, that is part of MATLAB, by Mathworks[®]. The underlying linear algebraic systems to be solved at each time step of `ode15s` have matrices that can be decomposed in the form

$$A = M_{nl} - \delta t \cdot a \cdot J, \quad (35)$$

where M_{nl} is the mass matrix, δt is the actual time step, J is the Jacobian matrix, and a is a constant. In our setting, the Jacobian matrix J is constant. On the other hand, we stress that the mass matrix M_{nl} is not and does depend on the solution, i.e., on the BM position ξ . Moreover, the formal expression of M_{nl} in Eqs. (26), (30), and (35) includes the inverse of matrix function B (lower bidiagonal, changing with the solution ξ at each time step) and of the matrix F (tridiagonal, constant, generated by the five-point finite-difference discretization of the Laplacian) that are full matrices; i.e., all entries of B^{-1} , F^{-1} are different from zero. Therefore, in order to avoid full coupling of the differential systems (26), requiring a computational cost per time step of $O((2N)^3)$ and a storage for $O(N^2)$ double precision floating point entries, we should not invert any matrix explicitly. Unfortunately, due to the nature of the matrix A in Eq. (35) as a sum of two components, we cannot use direct solvers for the linear systems of the form $Ax = b$. A popular way to approach this is the use of fixed-point iteration algorithms, as in Kim and Xin, 2005. However, fixed-point iteration algorithms converge slowly and often impose restrictions on the parameters of the model for convergence. In particular, artificial restrictions on the time step and/or on the admitted values of some parameters are an issue and this was the case for Kim and Xin (2005) approach, see Bertaccini and Fanelli, 2009 for a way to overcome this. In view of this, we propose here the use of iterative Krylov subspace solvers as the core solver for the linear algebraic systems with matrices as in Eq. (35). Indeed, by using iterative Krylov subspace solvers, we are able to lower the computational cost per step to at most linear in N (the number of mesh points on the BM). We recall that working with iterative Krylov subspace solvers does not require forming or storing the matrix A or its intermediate components. It is enough to access A through matrix-vector products, e.g., there is no need to form M_{nl} . The only requirement is to provide a fast procedure that, given a vector v , computes the vector

$$w = A \cdot v, \quad (36)$$

and the operation (36) is performed at each iteration of the Krylov solvers. Therefore, the operation (36) becomes the core “outer” operation in the solution of the underlying discretized model and it is performed through the solution of several “inner” steps, consisting in the solution of two sparse linear systems by sparse direct methods and in some other matrix-vector products and linear combinations of vectors. We experienced that the Krylov subspace iterative solver chosen, GMRES, converges to the required tolerance within a moderate average number of iterations that does not increase with N , the mesh size on the BM. More details on the technical solutions adopted and an analysis of the convergence process will be given in a forthcoming paper.

IV. RESULTS

In this section, we present some preliminary results to show that the nonlinear and non-local model described in Sec. II B, fully discretized and optimized in Sec. II C, may become, after having been tuned by careful comparison with the experimental available data, a useful complement to future experiments, to study some of the OAE issues mentioned in Sec. III. In the following, we show that the model is able to produce OAEs as a response to both impulsive (TEOAEs) and stationary stimuli (DPOAEs). The simulated TEOAEs show the expected time-frequency behavior, with shorter latency at higher frequency, consistent with the hypothesis that their backward transmission is associated with a slow transverse TW on the BM. The DPOAE components are produced at the cochlear places predicted by the theory after the corresponding forward transmission delays.

A. TEOAEs

The result of a numerical simulation ($N=1000$ partitions) using a broad-band click stimulus (level corresponding to 80 dB pSPL, duration of 80 μ s in the ear canal, similar to that routinely used in the clinical practice) is shown in Fig. 1(a), where we plot the computed BM transverse displacement as a function of time (in a 20 ms interval) and cochlear position x . One could choose to plot the BM velocity instead of displacement, obtaining a different vertical shape, due to the factor ω , which would amplify the basal part of the TW. From the top view shown in Fig. 1(b), the expected relation between the forward transmission time delay (BM forward delay) and the position $x(\omega)$ of the tonotopic resonant place of each frequency component ω is more clearly visible. This relation may be converted into a relation between BM delay and frequency using the Greenwood map (Greenwood, 1990).

Including randomly distributed mechanical irregularities (roughness) as spatial stiffness variations in relative amplitude $\varepsilon=0.05$, the click stimulus produces the delayed response at the stapes shown (for a total time of 50 ms) in Fig. 2 (the data are windowed to cancel the stimulus and to allow spectral analysis). This response would be transmitted back through the middle ear producing a TEOAE in the ear canal. A high level of fluctuations is used in the example to get a

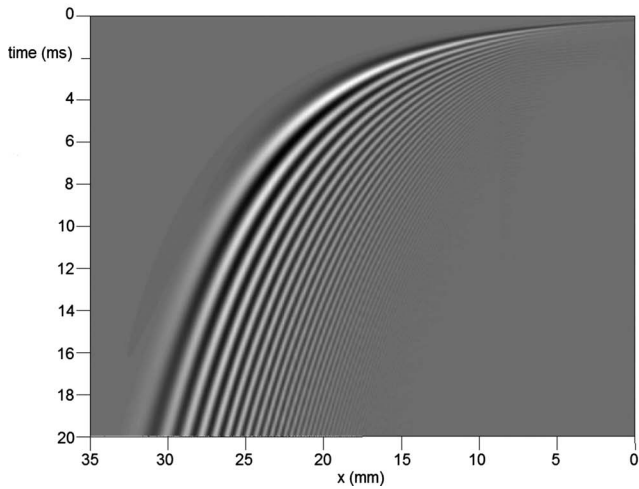
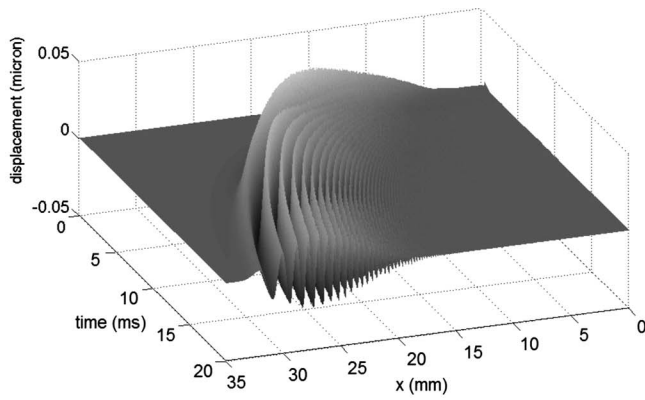


FIG. 1. BM response to a broad-band pulse (an 80 dB pSPL click of duration 80 μ s), as a function of time and cochlear longitudinal position x .

strong TEOAE signal. The waveform of Fig. 2 has been analyzed using time-frequency wavelet techniques to estimate the time delay of each frequency component. This delay closely corresponds to that of the TEOAE that would be measured in the ear canal because the delay introduced by the middle ear transmission, neglected in this model, is negligible (of order 100–200 μ s). The TEOAE wavelet delay

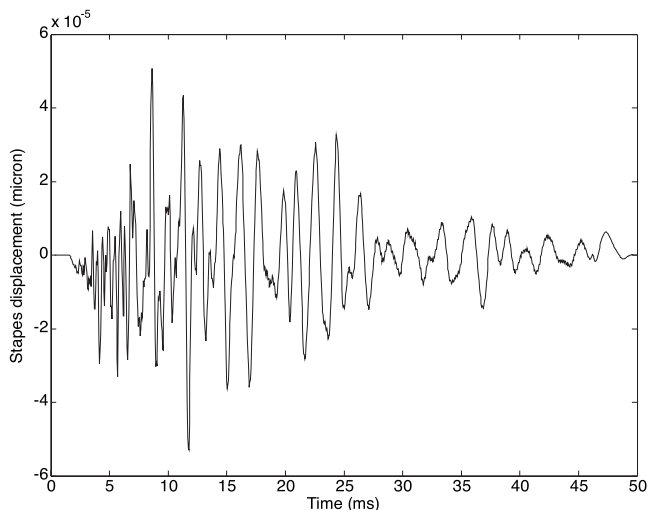


FIG. 2. “Otoacoustic” response computed at the stapes for 50 ms after the click, corresponding to the cochlear activation pattern of Fig. 1.

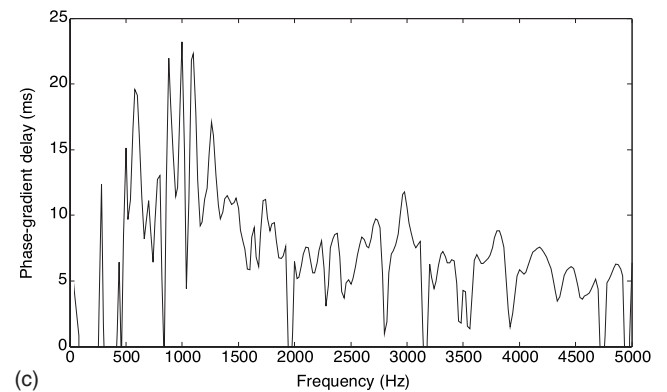
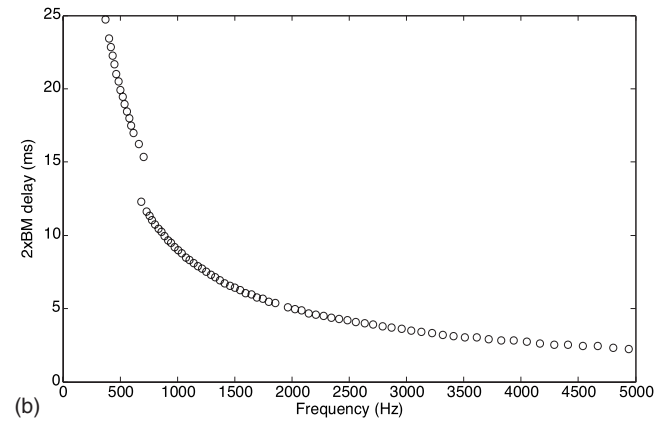
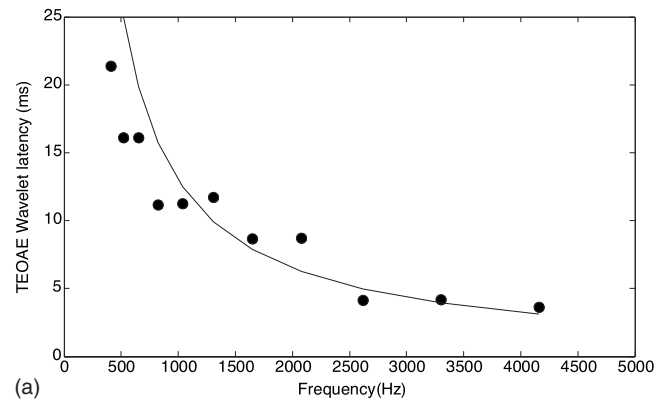


FIG. 3. Wavelet analysis estimate of the latency/frequency relation (a) of the response at the base of Fig. 2, compared to twice the delay of the BM response at each tonotopic place (b) and to the phase-gradient delay measured from the FFT of the same waveform (c).

computed for the waveform of Fig. 2 is shown in Fig. 3(a). In Fig. 3(b), we show twice the BM forward latency, estimated from Fig. 1(b) as the time of the maximum BM excitation and attributed to the frequency that is the best frequency for each place according to the Greenwood map (Greenwood, 1990). In Fig. 3(c), we show the phase-gradient delay estimated from the slope of the fast Fourier transform (FFT) phase. The good agreement confirms that the signal observed at the stapes comes from a backward slow TW on the BM, generated, for each frequency component of the stimulus, near its resonant place. In this model, the backward wave is generated by linear reflection from roughness. Indeed, the same simulation without roughness (not shown) produces no “OAE” response at the stapes. We note that the

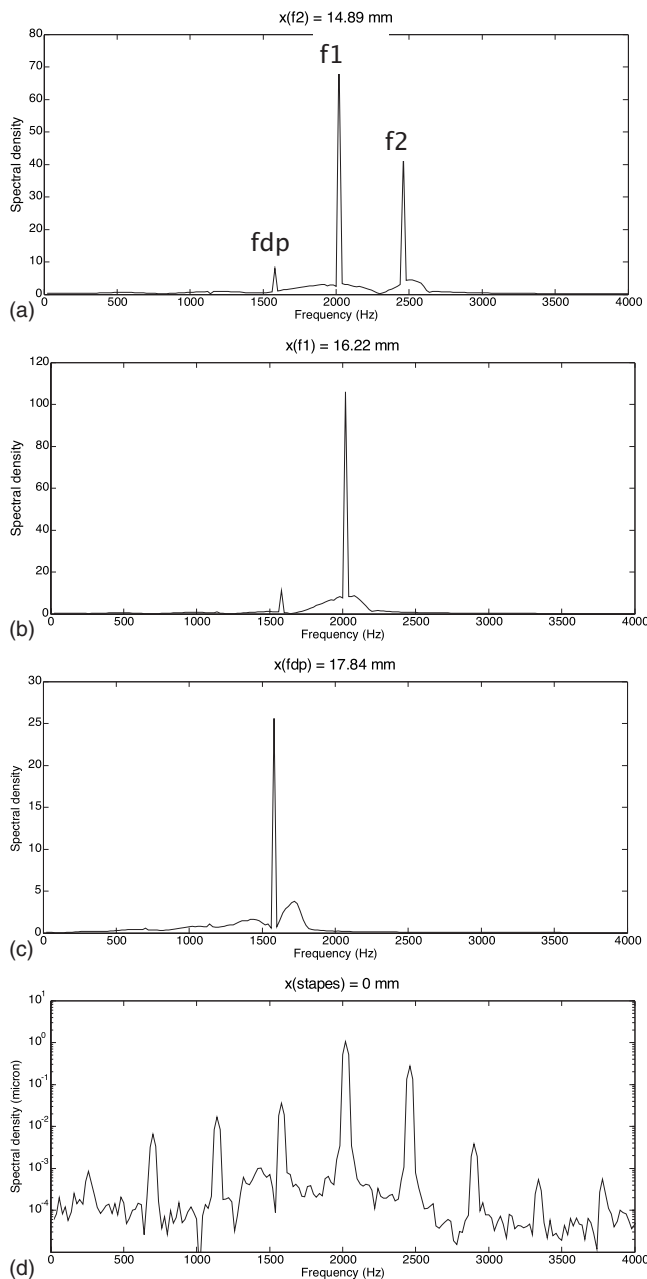


FIG. 4. Generation of the $2f_2-f_1$ distortion product due to nonlinear interaction of two primary tones ($f_1=2000$ Hz, $f_2/f_1=1.22$). The distortion tone is generated at $x(f_2)$ (a), its amplitude constantly increases reaching first $x(f_1)$ (b), and then $x(f_{DP})$ (c). The response at the stapes includes several other DP lines (d).

time-domain solution permits a direct estimate of the response waveform at the base (and at all other cochlear places) allowing us to compute time delays directly, without any assumption about the linearity of the system.

B. DPOAEs

In Fig. 4, we show the generation of the $2f_1-f_2$ distortion product due to nonlinear interaction of two primary tones ($f_1=2000$ Hz, $f_2/f_1=1.22$, $L_1-L_2=10$ dB, and $L_2=60$ dB SPL). In Fig. 4, the spectrum of the cochlear displacement is shown at different cochlear positions. The two primary tones propagate up to $x(f_2)$, where the DPOAE is generated and the f_2 tone is absorbed (and partially reflected

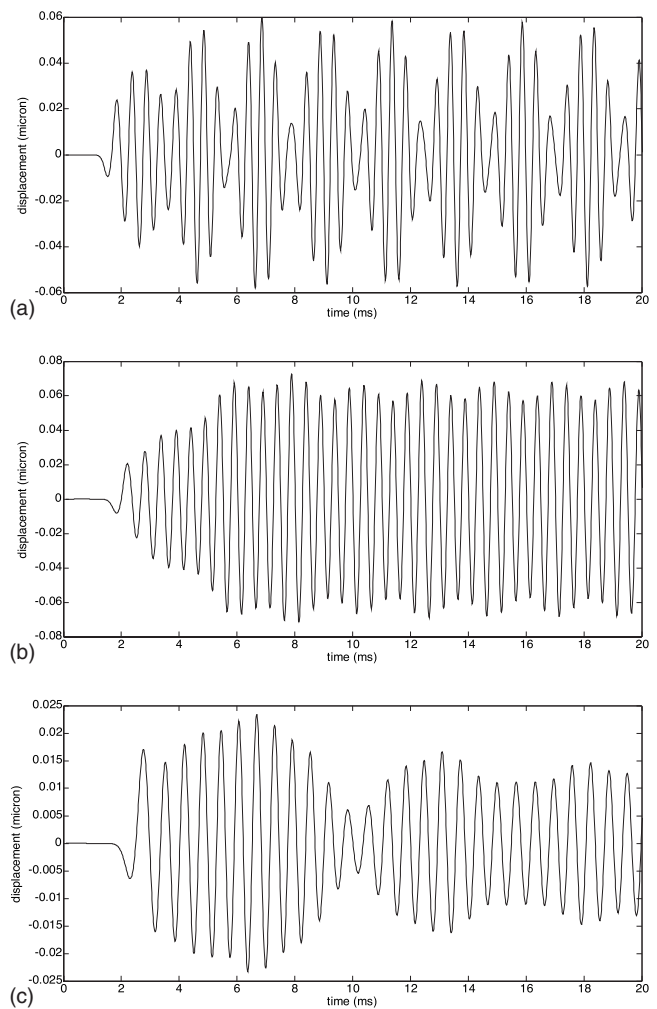


FIG. 5. Time evolution of the cochlear response at the three cochlear places of Figs. 4(a)–4(c).

by roughness) [Fig. 4(a)], then the f_1 tone is absorbed (and partially reflected by roughness) at its resonant place [Fig. 4(b)], whereas the distortion tone propagates forward to its tonotopic place, where it is amplified [Fig. 4(c)], absorbed, and partially reflected by roughness. The continuum spectrum, shifting to lower frequencies with increasing x , which can be observed below the spectral lines, is due to a small spurious broad-band TW. Several distortion product lines are visible in the spectrum of the response at the stapes [Fig. 4(d)], the most intense being that of frequency $f_{DP}=2f_1-f_2$, which is about 30 dB below the primary stimulus level. These DP levels are rather high, which is an indication that the parameters of the model still need to be optimized. At the present stage, a high level of DPOAE response may help show the qualitative behavior of the model.

The time-domain solution allows one to follow the generation of the DPOAE response also looking at displacement at fixed cochlear positions x as a function of time or at fixed times as a function of the position x . At the same three cochlear places of Figs. 4(a)–4(c), one gets the time evolution shown in Figs. 5(a)–5(c). From these plots, one can visually appreciate the different onset times of the response at different cochlear positions and the different frequency contents of the signal.

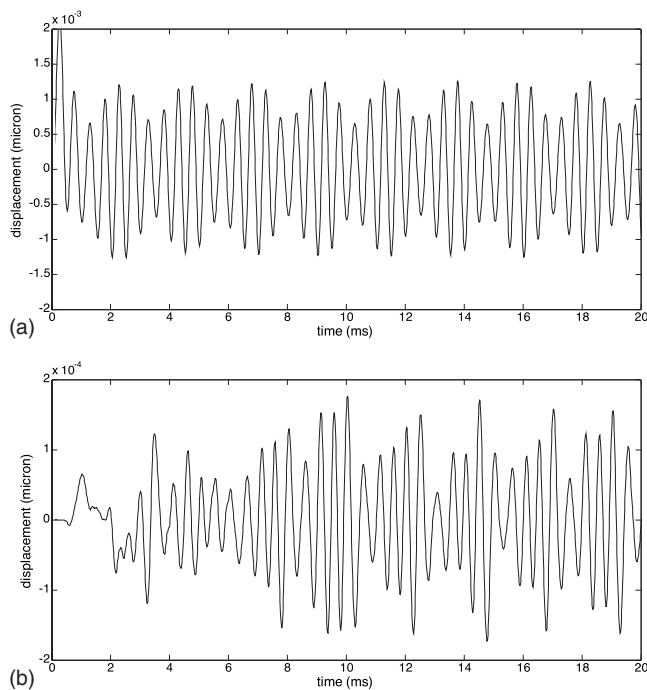


FIG. 6. Response at the stapes of the simulation shown in Fig. 4, which is obviously dominated by the stationary intense primary tones (a). Performing an identical simulation in which the nonlinear distortion term was suppressed in the region around $x(f_2)$ and subtracting the two response waveforms at the stapes, one can directly appreciate the onset delay of the DP at the base in the time domain (b).

In Fig. 6(a), we show the time-domain response at the stapes, which is obviously dominated by the intense primary tones. Performing an identical simulation in which the nonlinear distortion term is suppressed in the region around $x(f_2)$ and subtracting the two response waveforms, one can cancel the contribution from the stimuli and appreciate the onset delay of the DP at the base in the time domain [Fig. 6(b), note that the scale is ten times smaller than that in Fig. 6(a)]. The observed onset delay is compatible with the forward transmission delay of the primaries from the base to $x(f_2)$ estimated from the TEOAE simulation, plus a shorter backward transmission delay of the DP, as predicted by theory, and similar to what has been actually observed by experimental studies of the DPOAE onset time (Whitehead *et al.*, 1996). The backward delay is expected to be shorter, as explained in Sec. II, because the frequency of the DP is lower than the characteristic frequencies of the backward cochlear path; therefore, its propagation is faster than that of the f_2 tone along the same forward path. Slightly later, a contribution of the primary tones from their tonotopic places is expected to reach the base. This contribution is not canceled by the subtraction technique because, having suppressed nonlinear damping in the second simulation, the f_1 and f_2 components do not cancel exactly. The DPOAE contribution from the second source would come back even later, due to its lower frequency and level.

V. CONCLUSIONS

The multi-iterative computational strategies used within a stable time-step integrator based on implicit formulas con-

sidered in this study allowed us to solve accurately and efficiently our full cochlear model in the time domain. This is important in order to study the characteristic time delays associated with the propagation of acoustic signals along the BM, removing the ambiguities associated with the use of frequency-domain formulations, which are fully meaningful only for linear systems. A new 1D model, including feed-forward nonlinear and non-local terms, as well as cochlear roughness and a middle ear equation, has been implemented in a matrix formulation scheme, proposed by Elliott *et al.* (2007).

The results show that several aspects of the OAE phenomenology can be effectively predicted by such a model formulation, and help to design specific experiments dedicated to the study of a specific issue. In particular, the TEOAE latency/frequency relation is predicted in fine agreement with experimental data, and the DPOAE onset latency is shown to be associated with the BM forward and backward transmission delays, with results comparable to those of experimental studies on the DPOAE onset time.

Some parameters of the proposed continuous full cochlear model still need to be refined and tuned with an accurate comparison of its prediction with all available experimental data. After that, this model formulation can be extensively used to design experimental campaigns and diagnostic techniques, and to interpret the results of new experiments.

- Abdala, C., and Folsom, R. C. (1995). "Frequency contribution to the click-evoked auditory brain-stem response in human adults and infants," *J. Acoust. Soc. Am.* **97**, 2394–2404.
- Bertaccini, D., and Fanelli, S. (2009). "Computational and conditioning issues of a discrete model for sensorineural hypoacusia," *Appl. Numer. Math.* **59**, 1989–2001.
- Choi, Y., Lee, S., Parham, K., Neely, S. T., and Kim, D. O. (2008). "Stimulus-frequency otoacoustic emissions: Measurements and simulations with an active cochlear model," *J. Acoust. Soc. Am.* **123**, 2651–2669.
- de Boer, E., and Nuttall, A. L. (2003). "Properties of amplifying elements in the cochlea," in *Biophysics of the Cochlea: From Molecules to Models*, edited by A. W. Gummer (World Scientific, Singapore), pp. 331–342.
- de Boer, E., Zheng, J., Porsov, E., and Nuttall, A. L. (2008). "Inverted direction of wave propagation (IDWP) in the cochlea," *J. Acoust. Soc. Am.* **123**, 1513–1521.
- Don, M., Ponton, C. W., Eggermont, J. J., and Masuda, A. (1993). "Gender differences in cochlear response time: An explanation for gender amplitude differences in the unmasked auditory brainstem response," *J. Acoust. Soc. Am.* **94**, 2135–2148.
- Donaldson, G. S., and Ruth, R. A. (1993). "Derived band auditory brainstem response estimates of traveling wave velocity in humans. I: Normal-hearing subjects," *J. Acoust. Soc. Am.* **93**, 940–951.
- Dong, W., and Olson, E. S. (2008). "Evidence for reverse cochlear traveling waves," *J. Acoust. Soc. Am.* **123**, 222–240.
- Eggermont, J. J., and Don, M. (1980). "Analysis of the click-evoked brainstem potentials in humans using high-pass noise masking. II. Effect of click intensity," *J. Acoust. Soc. Am.* **68**, 1671–1675.
- Elliott, S. J., Ku, E. M., and Lineton, B. (2007). "A state space model for cochlear mechanics," *J. Acoust. Soc. Am.* **122**, 2759–2771.
- Furst, M., and Lapid, M. (1988). "A cochlear model for acoustic emissions," *J. Acoust. Soc. Am.* **84**, 222–229.
- Glasberg, B. R., and Moore, B. C. J. (1990). "Derivation of auditory filter shapes from notched-noise data," *Hear. Res.* **47**, 103–138.
- Greenwood, D. D. (1990). "A cochlear frequency position function for several species—29 years later," *J. Acoust. Soc. Am.* **87**, 2592–2605.
- He, W., Nuttall, A. L., and Ren, T. (2007). "Two-tone distortion at different longitudinal locations on the basilar membrane," *Hear. Res.* **228**, 112–122.
- Jedrzejczak, W. W., Blinowska, K. J., Konopka, W., Grzanka, A., and Durka, P. J. (2004). "Identification of otoacoustic emission components by

- means of adaptive approximations," *J. Acoust. Soc. Am.* **115**, 2148–2158.
- Kim, J., and Xin, J. (2005). "A two-dimensional nonlinear nonlocal feed-forward cochlear model and time domain computation of multitone interactions," *Multiscale Model. Simul.* **4**, 664–690.
- Lim, K. M., and Steele, C. R. (2002). "A three-dimensional nonlinear active cochlear model analyzed by the WKB-numeric method," *Hear. Res.* **170**, 190–205.
- Long, G. R., Talmadge, C. L., and Lee, J. (2008). "Measuring distortion product otoacoustic emissions using continuously sweeping primaries," *J. Acoust. Soc. Am.* **124**, 1613–1626.
- Moleti, A., and Sisto, R. (2003). "Objective estimates of cochlear tuning by otoacoustic emission analysis," *J. Acoust. Soc. Am.* **113**, 423–429.
- Neely, S. T., and Kim, D. O. (1986). "A model for active elements in cochlear biomechanics," *J. Acoust. Soc. Am.* **79**, 1472–1480.
- Neely, S. T., Norton, S. J., Gorga, M. P., and Jesteadt, W. (1988). "Latency of auditory brain-stem responses and otoacoustic emissions using tone-burst stimuli," *J. Acoust. Soc. Am.* **83**, 652–656.
- Nobili, R., and Mammano, F. (1996). "Biophysics of the cochlea II: Stationary nonlinear phenomenology," *J. Acoust. Soc. Am.* **99**, 2244–2255.
- Prijs, V. F., Schneider, S., and Schoonhoven, R. (2000). "Group delays of distortion product otoacoustic emissions: Relating delays measured with f1- and f2-sweep paradigms," *J. Acoust. Soc. Am.* **107**, 3298–3307.
- Probst, R., Lonsbury-Martin, B. L., and Martin, G. K. (1991). "A review of otoacoustic emissions," *J. Acoust. Soc. Am.* **89**, 2027–2067.
- Puria, S. (2003). "Measurements of human middle ear forward and reverse acoustics: Implications for otoacoustic emissions," *J. Acoust. Soc. Am.* **113**, 2773–2789.
- Ren, T. (2004). "Reverse propagation of sound in the gerbil cochlea," *Nat. Neurosci.* **7**, 333–334.
- Rhode, W. S. (1971). "Observations of the vibration of the basilar membrane in squirrel monkeys using the Mössbauer technique," *J. Acoust. Soc. Am.* **49**, 1218–1231.
- Schoonhoven, R., Prijs, V. F., and Schneider, S. (2001). "DPOAE group delays versus electrophysiological measures of cochlear delay in normal human ears," *J. Acoust. Soc. Am.* **109**, 1503–1512.
- Shera, C. A., and Guinan, J. J., Jr. (1999). "Evoked otoacoustic emissions arise from two fundamentally different mechanisms: A taxonomy for mammalian OAEs," *J. Acoust. Soc. Am.* **105**, 782–798.
- Shera, C. A., and Guinan, J. J., Jr. (2003). "Stimulus-frequency emission group delay: A test of coherent reflection filtering and a window on cochlear tuning," *J. Acoust. Soc. Am.* **113**, 2762–2772.
- Shera, C. A., Guinan, J. J., Jr., and Oxenham, A. J. (2002). "Revised estimates of human cochlear tuning from otoacoustic and behavioral measurements," *Proc. Natl. Acad. Sci.* **99**, 3318–3323.
- Shera, C. A., Tubis, A., and Talmadge, C. L. (2005). "Coherent reflection in a two-dimensional cochlea: Short-wave versus long-wave scattering in the generation of reflection-source otoacoustic emissions," *J. Acoust. Soc. Am.* **118**, 287–313.
- Shera, C. A., Tubis, A., and Talmadge, C. L. (2006). "Delays of SFOAEs and cochlear vibrations support the theory of coherent reflection filtering," Association for Research in Otolaryngology 2006 Meeting Poster.
- Shera, C. A., Tubis, A., Talmadge, C. L., de Boer, E., Fahey, P. F., and Guinan, J. J., Jr. (2007). "Allen–Fahey and related experiments support the predominance of cochlear slow-wave otoacoustic emissions," *J. Acoust. Soc. Am.* **121**, 1564–1575.
- Shera, C. A., and Zweig, G. (1991). "Reflection of retrograde waves within the cochlea and at the stapes," *J. Acoust. Soc. Am.* **89**, 1290–1305.
- Siegel, J. H., Cerka, A. J., Recio-Spinoso, A., Temchin, A. N., van Dijk, P., and Ruggero, M. A. (2005). "Delays of stimulus-frequency otoacoustic emissions and cochlear vibrations contradict the theory of coherent reflection filtering," *J. Acoust. Soc. Am.* **118**, 2434–2443.
- Sisto, R., and Moleti, A. (2002). "On the frequency dependence of the otoacoustic emission latency in hypoacoustic and normal ears," *J. Acoust. Soc. Am.* **111**, 297–308.
- Sisto, R., and Moleti, A. (2007). "Transient evoked otoacoustic emission latency and cochlear tuning at different stimulus levels," *J. Acoust. Soc. Am.* **122**, 2183–2190.
- Sisto, R., Moleti, A., and Shera, C. A. (2007). "Cochlear reflectivity in transmission-line models and otoacoustic emission characteristic time delays," *J. Acoust. Soc. Am.* **122**, 3554–3561.
- Talmadge, C. L., Tubis, A., Long, G. R., and Piskorski, P. (1998). "Modeling otoacoustic emission and hearing threshold fine structures," *J. Acoust. Soc. Am.* **104**, 1517–1543.
- Talmadge, C. L., Tubis, A., Long, G. R., and Tong, C. (2000). "Modeling the combined effect of basilar membrane nonlinearity and roughness on stimulus frequency otoacoustic emission fine structure," *J. Acoust. Soc. Am.* **108**, 2911–2932.
- Tognola, G., Ravazzani, P., and Grandori, F. (1997). "Time-frequency distributions of click-evoked otoacoustic emissions," *Hear. Res.* **106**, 112–122.
- Unoki, M., Miyauchi, R., and Tan, C.-T. (2007). "Estimates of tuning of auditory filter using simultaneous and forward notched-noise masking," in *Hearing—From Sensory Processing to Perception*, edited by B. Kollmeier, G. Klump, V. Hohmann, U. Langemann, M. Mauermann, S. Upenkamp, and J. Verhey (Springer, Berlin), pp. 19–26.
- Voss, S. E., and Shera, C. A. (2004). "Simultaneous measurement of middle-ear input impedance and forward/reverse transmission in cat," *J. Acoust. Soc. Am.* **116**, 2187–2198.
- Whitehead, M. L., Stagner, B. B., Martin, G. K., and Lonsbury-Martin, B. L. (1996). "Visualization of the onset of distortion-product otoacoustic emissions, and measurement of their latency," *J. Acoust. Soc. Am.* **100**, 1663–1679.
- Zweig, G., and Shera, C. A. (1995). "The origin of periodicity in the spectrum of otoacoustic emissions," *J. Acoust. Soc. Am.* **98**, 2018–2047.